Design and Voluntary Control of Variable Stiffness Exoskeleton Based on sEMG Driven Model

Yanghui Zhu, Qingcong Wu, *Member, IEEE*, Bai Chen, *Member, IEEE*, and Ziyue Zhao

***Abstract*—Exoskeleton robots are an exciting potential solution for patients with motor dysfunction to restore their daily activities. This paper introduces a variable stiffness exoskeleton robot (VSA-EXO) with variable stiffness actuators and a voluntary control strategy based on sEMG sensing. A sEMG-driven musculoskeletal model estimates joint torque and quasi-stiffness of the human joint through the sEMG signals of some muscles related to the joint. The voluntary control strategy adjusts the degree of assistance according to these detected voluntary efforts of the subjects, and transfers the stiffness adjustment of the human joints to the exoskeleton joints. Unlike the traditional assist-as-needed (ANN), this voluntary control strategy does not need to define a trajectory. Feasibility is demonstrated experimentally using three healthy subjects. Calibration experiments for the musculoskeletal model show that the NRMSE of the estimated torque and the actual torque of the three subjects are lower than 7.21%, proving the effectiveness of the musculoskeletal model. When using the exoskeleton assistance, with an assistance ratio of 0.3, the subjects' effort is reduced by up to 25.32%.**

***Index Terms*—Muscle strength estimation, Rehabilitation exoskeleton, Surface electromyography (sEMG), Variable stiffness actuator (VSA), Voluntary control.**

I. Introduction

RECENTLY, patients with lower limb motor dysfunction caused by diseases such as stroke, spinal cord injury, and muscle weakness are increasing [1]. Exoskeleton robots are a feasible solution for patients with motor dysfunction to restore their daily activities [2]. The exoskeletons are not only suitable for rehabilitation training of patients with motor dysfunction, but also for assisting their activities of daily living (ADL) [3]. The safety and comfort of the exoskeletons are the primary consideration factors for users [4], which are reflected in both mechanical structure and control.

Traditional exoskeleton robots are usually driven by actuators with high reduction ratios, which can achieve precise position control, such as ReWalk [5], HAL [6], and eLEGS [7]. However, a high reduction ratio will result in a high output impedance, making it difficult for users to drive the exoskeleton in reverse without continuous control [8]. In particular, the safety of the user cannot be guaranteed when the sensor fails. As an improvement, the researchers developed the series elastic actuator (SEA) for exoskeletons [9]. The SEA exhibits low output impedance and transparent force control performance in physical human-robot interaction (pHRI), but the control bandwidth of SEAs is limited [10]. Recently, variable stiffness actuators (VSA) have been developed [11], including antagonistic VSAs [12], variable transmission ratio VSAs [13]-[14] and variable preload type VSAs [15]-[16]. In these systems, the stiffness of the VSAs can be changed by adjusting the mechanical parameters or by the controller (impedance control, etc.) or by combining the two methods [31]. In exoskeleton applications, the variable stiffness characteristics of VSAs can allow the exoskeleton to imitate the stiffness adjustment skills of the human joints to improve performance, such as absorbing impact and reducing energy consumption [17]-[18].

The robotic equipment is used to receive sensor information and provide assistance based on the high-level control of the sensory information, which is called control strategy [19]. At present, different control strategies have been proposed for rehabilitation training, mainly including passive training and active training [32]. Passive training usually assists patients to track a predetermined trajectory designed to aid rehabilitation [20]. This control strategy is beneficial for neuroplasticity rehabilitation training of patients with severe motor dysfunction. In fact, for patients with voluntary exercise ability, active training is more effective for exercise recovery [21]. The assist-as-need (AAN) control can provide different levels of assistance based on the patient's effort. Hussain et al. achieve AAN by adaptive impedance control [22], where the impedance parameters are adjusted according to the voluntary effort of the patient. However, the patient's voluntary effort is calculated through interactive force sensors and dynamic

Manuscript received January, 18, 2022; Accepted March, 3, 2022. This letter was recommended for publication by Editor Jee-Hwan Ryu upon evaluation of the Associate Editor and Reviewers' comments. This work was supported in part by the National Natural Science Foundation of China (Grant No. 52175014), in part by the Natural Science Foundation of Jiangsu Province (Grant No. BK20211183), in part by the CIE-Tencent Robotics X Rhino-Bird Focused Research Program (Grant No. 2020-01-008) and in part by the Innovation Project of Nanjing University of Aeronautics and Astronautics(Grant No.xcxjh20210505). (Corresponding author: Qingcong Wu and Bai Chen.)

Yanghui Zhu, Qingcong Wu, Bai Chen and Ziyue Zhao are with the College of Mechanical and Electrical Engineering, Nanjing University of Aeronautics and Astronautics, Nanjing 210016, Jiangsu, China (email: zhuyanghui@nuaa.edu.cn;wuqc@nuaa.edu.cn;chenbye@nuaa.edu.cn; zhaozy@nuaa.edu.cn).

Digital Object Identifier (DOI): see top of this page.

models, which increases the complexity of the system. Gui et al. designed a progressive AAN controller [23], which can estimate the patient's voluntary torque based on the patient's electromyogram (EMG) to provide the required assistance. The ANN control strategy involves the voluntary efforts of the patient, but the controller still needs to set the trajectory, and is not suitable for assisting the patient's ADL. Voluntary control is a feasible solution, which provides torque assistance in an open loop based on the patient's voluntary effort, and is not limited by the patient's motion trajectory. Surface electromyography (sEMG) is a biological signal generated by nerve transmission before muscle contraction, which can be used to estimate the voluntary effort of the human body [24]. In addition, considering the impedance characteristics of muscles and tendons, the sEMG can be further used to estimate the stiffness of human joints [25]. However, this method needs to obtain sEMG signals of all muscles related to joint movement, which is difficult in actual operation.

This work aims to develop a variable stiffness exoskeleton robotic system (VSA-EXO), and to conduct some experiments on the feasibility study before applying to patients. The main contributions of this paper include: 1) Based on the variable stiffness actuator [16], the mechanical structure of the VSA-EXO is designed. 2) This paper proposes a sEMG-driven musculoskeletal model that can estimate joint torque and quasi-stiffness through a small part of muscles. 3) This paper proposes a voluntary control strategy. In this control strategy, the exoskeleton can provide proportional assistance according to the voluntary movement of the human body, and the exoskeleton can imitate the quasi-stiffness adjustment skills of the human joints. As far as we know, this has not been reported. 4) Experiments are conducted on three healthy subjects, which proved the feasibility of the proposed control strategy to reduce the effort of the subjects, and provided a case for an exoskeleton with controllable torque.

II. VARIABLE STIFFNESS EXOSKELETON DESIGN

A. Variable stiffness mechanism

In the previous research, we proposed a reconfigurable variable stiffness actuator (RVSA) [16], the principle is shown in Fig. 1(a). Six sets of pulleys are arranged between the input panel and the output panel, and the pulley sets are connected by steel wire ropes. The steel wire rope and the tension spring constitute an elastic element. The preload of the spring can be adjusted by a reel. When the input panel is rotated, an elastic deflection angle is generated between the input panel and the output panel, and the output torque is generated on the output panel through the pulling force of the wire rope. The derivative of the output torque and the deflection angle is the output stiffness. In addition, the number of pulley blocks can be changed by changing the winding method of the wire rope to achieve reconstruction, which is described in detail in the literature [16]. The force of a single pulley of the RVSA is shown in Fig. 1(b). The quasi-static equation can be expressed by the following formula:

$$T = 4N^2Kac\sin\theta(1-(a-c)/\sqrt{a^2+c^2-2ac\cos\theta}) \\ +2NF_0ac\sin\theta/\sqrt{a^2+c^2-2ac\cos\theta}. \quad (1)$$

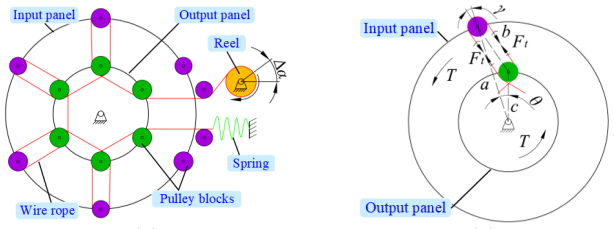

(a) (b)

Fig.1 Variable stiffness mechanism and force balance diagram. (a) Variable stiffness mechanism, (b) Quasi-static force balance diagram of a single pulley block.

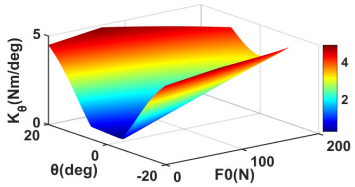

Fig.2 The relationship between the stiffness, the preload and the elastic deflection angle.

where T is the input torque, N is the number of pulleys, K is the equivalent linear stiffness of the elastic element, a and c are geometric parameters, and θ is the deflection angle (see Fig. 1(b)), F_0 is the preload of the spring.

The stiffness K_θ of the joint output can be expressed as:

$$K_\theta = \partial T / \partial\theta. \quad (2)$$

When the same deflection angle θ is generated, the greater the preload F_0, the greater the input torque T, that is, the greater the output stiffness K_θ. The output stiffness can be changed by adjusting the pretension F_0. This variable stiffness method can easily realize independent control of joint position and stiffness. In addition, within the same spring preload change range, the greater the number of pulley sets N, the greater the range of joint stiffness that can be changed. The reconfigurability of the RVSA can be used to improve the adjustable range of joint stiffness. In this paper, the parameters of the RVSA are set as: N=4, a=0.05m, c=0.035m, K=3814.2N/m, the relationship between stiffness, preload and elastic deflection angle is shown in Fig. 2.

B. Structural design of variable stiffness exoskeleton

The exoskeleton system we designed is for patients with moderate or mild motor dysfunction (stroke, muscle weakness, arthritis) who have a certain degree of active movement ability. Therefore, the variable stiffness exoskeleton (VSA-EXO) designed in this paper adopts a design method that combines active and passive joints. When the human body is walking, the knee joint is mainly used to support the human body, absorb the impact with the ground, and the stiffness changes significantly [33]. Therefore, the knee joint is designed as an active joint driven by the RVSA. The hip joint and ankle joint are spherical hinge joints with three degrees of freedom and are designed as passive joints. The degrees of freedom of the VSA-EXO include: abduction/adduction and extension/flexion of the hip joint; extension/flexion of the knee joint; abduction/adduction, inversion/eversion and dorsi/plantar flexion of the ankle joint, as shown in Table I. The range of motion of VSA-EXO can meet the subjects' daily walking, up and down stairs and other sports. The overall VSA-EXO is shown in Fig. 3(a), which mainly includes a waist drive module, a passive hip joint

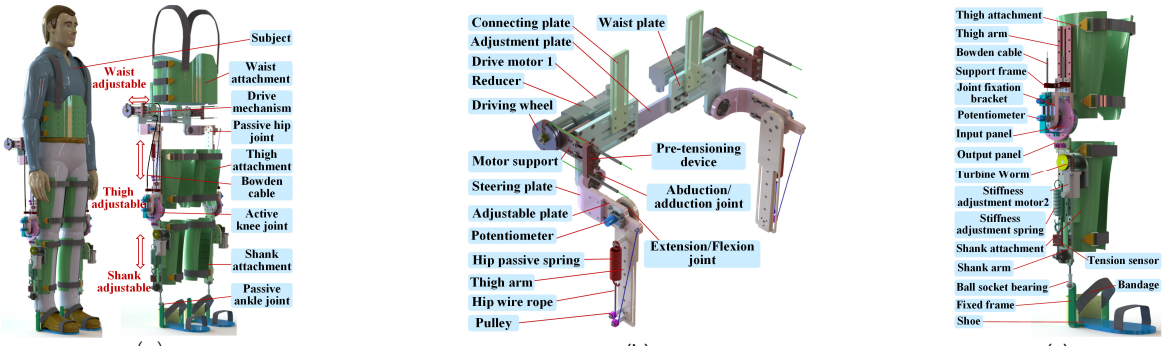

(a) (b) (c)

Fig.3 Three-dimensional structure of the VSA-EXO. (a) Overall view of the VSA-EXO. (b) The waist drive module and passive hip joint module. (c) The active knee joint module and passive ankle joint module.

TABLE I
THE RANGE OF MOTION OF VSA-EXO

Joint	Degree of freedom	Range of motion
Hip joint	Abduction/Adduction	-60°~60°
Hip joint	Extension/Flexion	-60°~85°
Knee joint	Extension/Flexion	-135°~0°
Ankle joint	Abduction/Adduction	-45°~45°
Ankle joint	Dorsi/Plantar flexion	-45°~45°
Ankle joint	Inversion/Eversion	-30°~30°

module, a variable stiffness drive knee joint module, a passive ankle joint module and a wearable module. Among them, the waist drive module places the distal Bowden cable drive mechanism. The passive hip joint module is equipped with a passive spring, which can store and release energy for walking. The variable stiffness drive knee joint module is driven by the variable stiffness actuator, which can realize exercise assistance. The passive ankle joint module is used to keep the exoskeleton from sliding down the leg. The wearable module is a component that connects the exoskeleton to the subject. The total mass of VSA-EXO is 7.6kg.

The waist drive module and the hip joint module are shown in Fig. 3(b). In the waist drive module, the height of the connecting plate and the width of the adjustment plate is adjustable to adapt to different subjects. The drive motor and the reducer are fixed on the motor support connected to the waist plate. The output shaft of the reducer is connected to the driving wheel through a key, and the driving wheel is connected to the inner wire rope of the Bowden cable. This connection mode can realize the remote transmission of force. In this design, the weight of the exoskeleton drive module is mainly supported by the shoulder strap.

The hip joint module includes passive abduction/adduction rotation joints and passive elastic extension/flexion rotation joints. The degrees of freedom of abduction/adduction and extension/flexion is realized by the structure of the bearing and the shaft. The front and back length of the adjustable plate can be adjusted in a small range to suit different subjects. In addition, the wire rope between the adjustable plate and the thigh arm is connected in series with the tension spring installed on the thigh arm. The configuration can store energy during the flexion phase of the human hip joint and release energy during the extension phase of the hip joint, enabling passive assistance [26]. The stage of energy storage and energy release of the spring can be determined by adjusting the initial tension position of the spring. The passive assistance energy efficiency has been put into practice in [27].

The knee joint module and the ankle joint module are shown in Fig. 3(c). The extension/flexion degree of freedom of the knee joint is driven by the RVSA. The outer layer of the Bowden cable is placed on the support frame connected to the thigh arm, and the inner steel wire of the Bowden cable is connected to the input panel, thereby transmitting the driving force of the remote drive mechanism to the input panel. The driving torque of the input panel and the output panel is transmitted through the steel wire rope and the pulley block. As a result, the corresponding driving torque is generated between the thigh arm of the knee joint and the shank arm. The position and stiffness of the knee joint can be independently controlled by two motors, where the motor M1 is used to control the output torque, and the motor M2 changes the spring preload F_0 to achieve stiffness control.

The main function of the ankle joint is to support the weight of the body, push forward and turn the body [33]. The traditional exoskeleton ankle joint only retains the degrees of freedom of dorsi/plantar flexion, which will cause the subject to be unable to rotate. The ankle joint consists of two ball socket bearings. One ball socket bearing is aligned with the ankle joint and connected to the fixed frame, and the other ball socket bearing is fixed and connected to the shank arm. This combination allows the ankle joint to have redundant degrees of freedom, which can reduce the discomfort caused by the dislocation of the exoskeleton joint and the ankle joint. The lower part of the fixed frame is fixed with the shoe to support the weight of the exoskeleton leg and keep the exoskeleton from slipping down the legs. The shoe is made of a composite of carbon fiber board and flexible rubber, which can achieve flexion/stretching of the toe.

C. Real-time control system

The control system of the VSA-EXO is shown in Fig. 4. The control system uses a hierarchical control method of the host computer (personal computer) and the target computer (IPC-610L, Advantech). The control code written in the host computer is sent to the target computer to run through IP communication. The data acquisition cards (PCL-818, Advantech and NI-6602, National Instruments) are integrated on the target computer to collect feedback signals from encoder (motor internal encoder), potentiometer (P3014-V1-Cw180, accuracy: 0.27°), sEMG sensor (AT-04-001), and tension sensor (JLBS-MD-50KG, accuracy: 0.1N). The collected data is filtered, calculated and solved in the target computer to obtain the control signal. The control signal is output to the

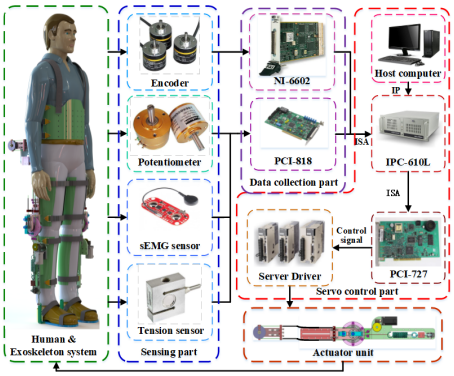

Fig.4 Schematic diagram of the exoskeleton real-time control system

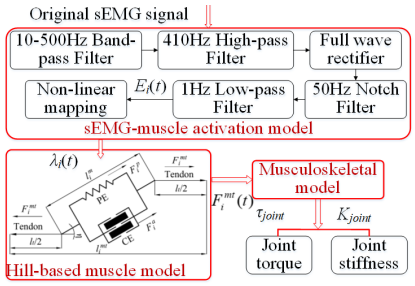

Fig.5 The diagram of the sEMG-driven musculoskeletal model

TABLE II
MUSCLE PARAMETERS

Muscle	$F_i^{\max}$ (N)	l_i^{m0} (m)	η_0 (rad)	c_{0i}	c_{1i}	c_{2i}	c_{3i}
BF	804	0.173	0.401	0.169	0.020	-0.013	-0.005
ST	410	0.201	0.0873	0.200	0.036	-0.015	-0.007
VM	1294	0.089	0.0873	0.044	-0.044	-0.002	0.001
VL	1871	0.084	0.0873	0.040	-0.042	0	0.002

driver of the servo motor through an analog output card (PCL-727, Advantech) to control the motor movement. Finally, the data are sent to the host computer via IP communication for recording. The sampling rate of the host computer and target computer of the control system are both set to 1kHz.

III. VOLUNTARY CONTROL SCHEME

A. sEMG-driven musculoskeletal model

The sEMG-driven musculoskeletal model developed in this paper is divided into sEMG-muscle activation model, Hill-based muscle model, and musculoskeletal model, as shown in Fig. 5.

1) sEMG-muscle activation model. The original sEMG signal has a lot of noise and cannot be used directly. This paper uses 10-500Hz band-pass filter, 410Hz high-pass filter, full-wave rectifier, 50Hz low-pass filter and 1Hz low-pass filter to filter the original signal. The activation of the muscle $\lambda_i(t)$ can be expressed as:

$$\lambda_i(t) = (e^{\xi E_i(t)} - 1) / (e^{\xi} - 1) \tag{3}$$

where $E_i(t)$ is the sEMG signal after filtering, and ξ is the constant that defines the curvature of the nonlinear mapping ($-3<\xi<0$).

2) Hill-based muscle model. In the Hill-based muscle model, the muscle is composed of muscle fibers and tendons in series. Muscle fibers are composed of active contraction element (CE) and passive elastic element (PE) in parallel. Therefore, the viscoelastic force produced by the muscle can be expressed as:

$$F_i^{mt} = (F_i^a + F_i^p)\cos\eta \tag{4}$$

where F_i^{mt} is muscle-tendon force, η is the pinnate, F_i^a and F_i^p are active muscle force and passive muscle force, respectively, which can be expressed as:

$$F_i^a = f_a(l_i) f_v(v_i) \lambda_i(t) F_i^{\max} \tag{5}$$

$$F_i^p = f_p(l_i) F_i^{\max} \tag{6}$$

where $f_a(l_i)$ and $f_p(l_i)$ are functions related to muscle length, l_i is the normalized muscle length, v_i is the normalized muscle contraction speed, and $F_i^{\max}$ is the maximum isometric muscle force. l_i and η can be expressed as:

$$l_i = l_i^m / l_i^{m0} \tag{7}$$

$$\eta = \arcsin(\sin(\eta_0) / l_i), \tag{8}$$

where l_i^{m0} is the optimal muscle length, l_i^m is the muscle length and η_0 is the optimal pinnate angle.

According to the literature [28], $f_a(l_i)$ and $f_p(l_i)$ can be expressed as:

$$f_a(l_i) = 0.9866 e^{-(l_i-\alpha_1)^2/\beta_1^2} + 0.6533 e^{-(l_i-\alpha_2)^2/\beta_2^2} \tag{9}$$

$$f_a(l_i) = 0.000065 e^{6.47 l_i}. \tag{10}$$

where α_1=1.073, α_2=0.7201, β_1=0.2952, β_2=0.1759.

The muscle length l_i^m is a function of the corresponding joint angle φ. The relationship between muscle length and angle can be fitted with a third-order polynomial, which is defined as follow:

$$l_i^m = c_{0i} + c_{1i}\varphi + c_{2i}\varphi^2 + c_{3i}\varphi^3 \tag{11}$$

where φ is the joint angle, and c_{0i}, c_{2i}, c_{3i} and c_{4i} are the coefficients of the polynomial.

The flexor muscles related to the knee joint include the biceps femoris (BF) muscle and the semitendinosus (ST) muscle, and the extensor muscles include the medial femoris (VM) and lateral femoris (VL). The corresponding parameters are shown in Table II. The data is obtained from OpenSim4.0 [29].

3) Musculoskeletal model. The torque of the muscle to the joint can be expressed by the product of the muscle force and the lever arm of the muscle.

$$\tau_i^m = F_i^{mt} r_i \tag{12}$$

where τ_i^m is the torque of the muscle to the joint, and r_i is the length of the lever arm, which can be calculated as

$$r_i = \partial l_i^m / \partial \varphi \tag{13}$$

The torque of the joint can be obtained by summing all the muscles acting on the joint (the torque produced by the extensor muscle is positive).

$$\tau_{joint} = \left|\sum \tau_i\right|_{\text{Extensor}} - \left|\sum \tau_i\right|_{\text{Flexor}} \tag{14}$$

However, in practical applications, all the muscle forces acting on the joints cannot be fully obtained. This paper uses a partial muscle force contribution to estimate joint torque. The joint torque can be expressed as

$$\tau_{joint} = \sigma_1 \left|\sum_{i=1}^{n_1} \tau_i\right|_{\text{Extensor}} - \sigma_2 \left|\sum_{i=1}^{n_2} \tau_i\right|_{\text{Flexor}} \tag{15}$$

where σ_1 and σ_2 are the contribution ratio coefficients of the extensors and flexors, respectively, which can be obtained through experimental calibration. n_1 and n_2 are the number of selected extensors and flexors, respectively.

It has been observed that the greater the joint torque, the greater the stiffness of the joint [30]. In addition, when the torque of the antagonist muscle increases at the same time, the joint torque will not increase, but the joint stiffness will increase. Therefore, we define a stiffness coefficient *STI*.

$$STI(t) = \sigma_1 \left| \sum_{i=1}^{n_1} \tau_i \right|_{\text{Extensor}} + \sigma_2 \left| \sum_{i=1}^{n_2} \tau_i \right|_{\text{Flexor}} \tag{16}$$

The joint stiffness can be expressed as

$$K_{joint} = k_1 STI(t) + k_0 \tag{17}$$

where k_1 (rad^{-1}) and k_0 (Nm/rad) are constants.

In practical applications, it is difficult to obtain accurate human joint stiffness. In this paper, we use the quasi-stiffness of the human joints to express the stiffness of the joints. It can be seen from (17) that the quasi-stiffness of human joints can be obtained through the stiffness coefficient *STI*.

B. Control Schemes

In this paper, the developed sEMG-driven musculoskeletal model is used to adjust the assistance torque and joint stiffness of the exoskeleton, as shown in Fig. 6. The control scheme includes two parts: torque control and stiffness control.

In the torque control loop, the human joint torque estimated by the sEMG-driven musculoskeletal model is scaled down and used as the reference input torque of the torque controller to assist the subject. The assistance torque can be expressed as:

$$T_{ref} = \omega \tau_{joint} \tag{18}$$

where T_{ref} is the reference torque of the torque controller, and ω is the auxiliary ratio coefficient, which can be adjusted according to the assistance needs.

The torque controller is composed of two cascade control loops. In the primary loop, the torque feedback signal of the exoskeleton joint is estimated by (1) ($T(\theta, F_0)$). The error between the reference input torque T_{ref} and the feedback torque T_{es} is modulated by the PID controller to generate the speed control signal of the motor. The control rate of the motor speed is:

$$v_1(t) = K_{p1} e_1(t) + K_{i1} \int_0^t e_1(t)dt + K_{d1}(de_1(t)/dt) \tag{19}$$

where $v_1(t)$ is the speed control rate of the drive motor M1, $e_1(t)=T_{ref}-T_{es}$, K_p, K_i and K_d are the proportional coefficient, differential coefficient and integral coefficient of the PID controller, respectively.

The secondary loop of the torque controller is the speed closed loop of the motor, which is controlled by the servo drive. The advantage of this torque control method is that it does not need to use an additional torque sensor to achieve torque control, and the effectiveness of the torque control method in the dynamic process has been verified in [16].

Human joints have been able to adapt to walking after tens of thousands of years of evolution, for example, human knee joint has high stiffness in the support stage of gait to improve joint response speed and absorb impact, and human knee joint has low stiffness in the swing stage of gait to improve leg flexibility [17]-[18]. In the voluntary control scheme in this paper, the

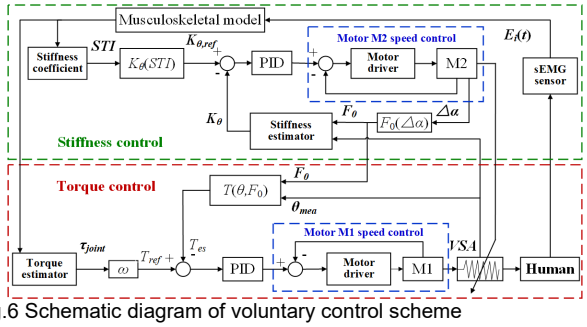

Fig.6 Schematic diagram of voluntary control scheme

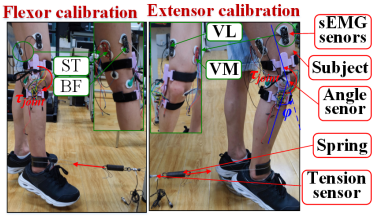

(a)

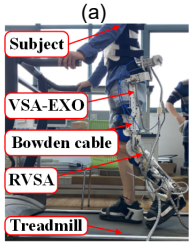

(b)

Fig.7 (a)The experimental setup for muscle calibration, in which the vertical state of the thigh and shank is defined as the zero position of the knee joint, and the extension is the positive direction. (b) The Voluntary gait assisted experiment device.

exoskeleton joints behave in the same way as human joints, so the exoskeleton stiffness is designed to be the quasi-stiffness of human joints. In the stiffness control loop, the stiffness coefficient *STI* obtained from the sEMG-driven musculoskeletal model is used to generate the reference input stiffness of the exoskeleton joint. Considering the variable range of exoskeleton stiffness, in this paper, the reference stiffness $K_\theta(STI)$ is obtained by the following equation:

$$K_\theta(STI) = K_{\theta,\min} \frac{|STI_{\max}| - sat(|STI|)}{|STI_{\max}|} + K_{\theta,\max} \frac{sat(|STI|)}{|STI_{\max}|} \tag{20}$$

where $K_{\theta,\min}$ and $K_{\theta,\max}$ are the minimum stiffness (60Nm/rad) and maximum stiffness (150Nm/rad) defined by the exoskeleton joint, and $STI_{\max}$ is the maximum stiffness coefficient obtained according to repeated experiments during walking. On the one hand, this stiffness-adjusting behavior can provide different passive compliance behaviors for the exoskeleton during the different gait phase (high force control bandwidth and response speed during the support phase of gait [11], and high compliance during the swing phase of gait to reduce the resistance of the exoskeleton when the human joints back-drive the exoskeleton). On the other hand, this stiffness-adjusting behavior can imitate human joints by changing the stiffness of the joints to absorb the impact of the exoskeleton's collision with the ground.

In addition, in the stiffness controller, the stiffness feedback signal is obtained by the stiffness estimator (equation (2)). The error between the reference stiffness and the estimated stiffness is modulated by the PID controller to generate the speed control

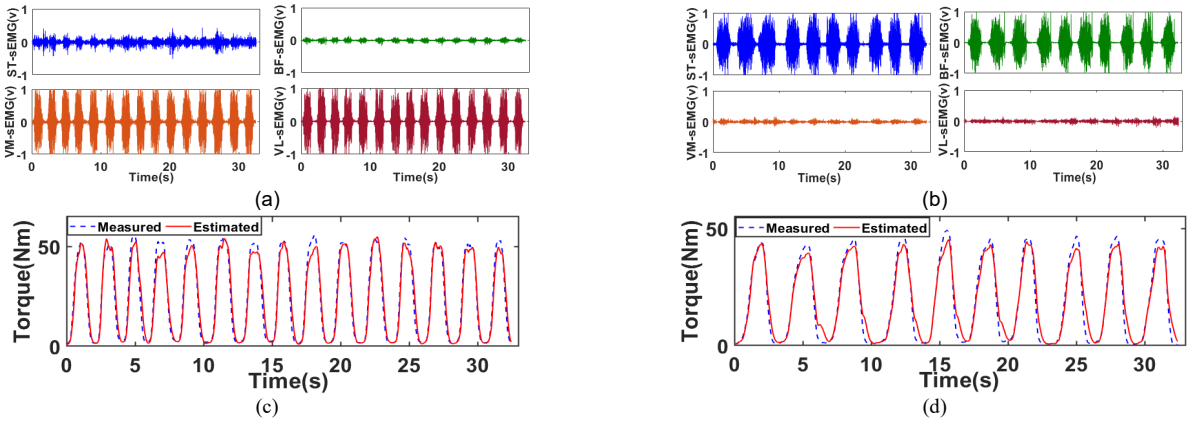

Fig.8 The calibration result of the musculoskeletal model of subject 1. (a) Subject 1's sEMG signal during flexor calibration. (b) Subject 1's sEMG signal during extensor calibration.(c) The estimated torque and measured torque for flexor calibration.(d) The estimated torque and measured torque for extensor calibration.

TABLE III
CALIBRATION RESULTS

Subject	Muscle	Contribution ratio	RMSE(Nm)	NRMSE	CC
Subject1	Extensor	1.3082	3.5499	7.21%	0.9848
	Flexor	1.6899	3.6735	6.61%	0.9835
Subject2	Extensor	1.4216	2.654	5.56%	0.9912
	Flexor	1.5365	3.0523	6.25%	0.9865
Subject3	Extensor	1.3658	1.8954	3.25%	0.9956
	Flexor	1.5672	2.1256	5.68%	0.9812

signal of the stiffness adjustment motor M2. The speed of the motor M2 is controlled by the internal speed closed loop of the servo drive. The real-time control of the joint stiffness is achieved by changing the spring preload F_0 (related to the position $\Delta\alpha$ of the reel). The relationship between the preload F_0 of the spring and the position of the reel can be expressed as:

$$F_0 = KR\Delta\alpha + F_{r0} \tag{21}$$

$$\Delta\alpha = \alpha_{m2} / \gamma \tag{22}$$

where R is the radius of the reel, F_{r0} is the initial preload of the spring when the reel is in the initial position, α_{m2} is the position of the motor M2, and γ is the reduction ratio.

IV. EXPERIMENTS AND RESULTS

A. Musculoskeletal model calibration experiments

In order to obtain the human joint torque τ_{joint} and the stiffness coefficient STI, the experimental calibration is required to obtain the contribution ratio coefficients σ_1 and σ_2 of the extensor and flexors. The calibration experiments are carried out on three healthy subjects (Subject 1: male, 70kg, 25 years old, 1.80m; Subject 2: male, 60kg, 24 years old, 1.71m; Subject 3: female, 50kg, 22 years old, 1.64m;). The experimental protocol has been approved by the review committee of Nanjing University of Aeronautics and Astronautics. In addition, the subjects have informed consent to participate in the experiment and signed a written agreement. The knee joints of these subjects are strapped in series with the tension sensor and the tension spring, as shown in Fig. 7(a). These subjects have sEMG sensors attached to the corresponding leg muscles BF, ST, VM, and VL to collect sEMG signals from the muscles. In the experiment, these subjects were asked to bend (stretch) the knee indirectly to complete the calibration of torque at different joint angles. The actual torque of the subject's joint is calculated by the tension sensor and the arm length of the shank. The vertical state of the thigh and shank is defined as the joint zero position, and the extension is the positive direction. The data and results of the muscle calibration process are shown in Fig. 8 and Table III. Fig. 8(a) and Fig. 8(b) are the sEMG signal and torque estimation results of Subject 1 during the flexor calibration process, respectively. Fig. 8(c) and Fig. 8(d) are the sEMG signal and torque estimation results of Subject 1 during the extensor calibration process, respectively. Table III is the calibration results of three subjects, where the contribution rate is σ_i (i=1,2, obtained by least squares fitting) in (15), the RMSE is the root mean square error, the NRMSE is the normalized root mean square error, and CC is the correlation coefficient. The RMSE of all subjects are less than 3.6735Nm, the NRMSE are less than 7.21%, and the correlation coefficients are greater than 0.9812, indicating that the torque estimation method based on sEMG is effective.

B. Voluntary gait assisted experiment

The voluntary gait assisted experiment setup is shown in Fig. 8(b). The subjects wear an exoskeleton to train on a treadmill. Five sets of experiments are conducted for each subject. Each subject carried out five sets of experiments, including the experiment of gait training on the treadmill with ω=0, 0.1, 0.2, 0.3 with the exoskeleton and the baseline experiment without the exoskeleton. In the experiment, the subjects all walk uniformly on the treadmill at a speed of 1m/s. The assistance efficiency of the exoskeleton is evaluated by calculating the root mean square (RMS) of the joint torque per unit mass, which is defined as follows:

$$RMS = \sqrt{1/N\sum_{i=1}^{N}\tau_i^2} \tag{23}$$

where τ_i represents the joint torque estimated by (15) at the i-th sampling time. To show the effect of the exoskeleton on the subject's joint torque, the subject does not wear the exoskeleton as the baseline. The assistance efficiency η is defined as:

$$\eta = (RMS_0 - RMS_\omega) / RMS_0 \tag{24}$$

where RMS_0 is the RMS when the subject is not wearing the exoskeleton, and RMS_ω is the RMS when the auxiliary ratio factor is ω.

The results of the voluntary gait assisted experiment are shown in Fig. 9. Fig. 9(a) shows the mean value and standard deviation (SD) of the knee joint angle for a single gait cycle of subject 1

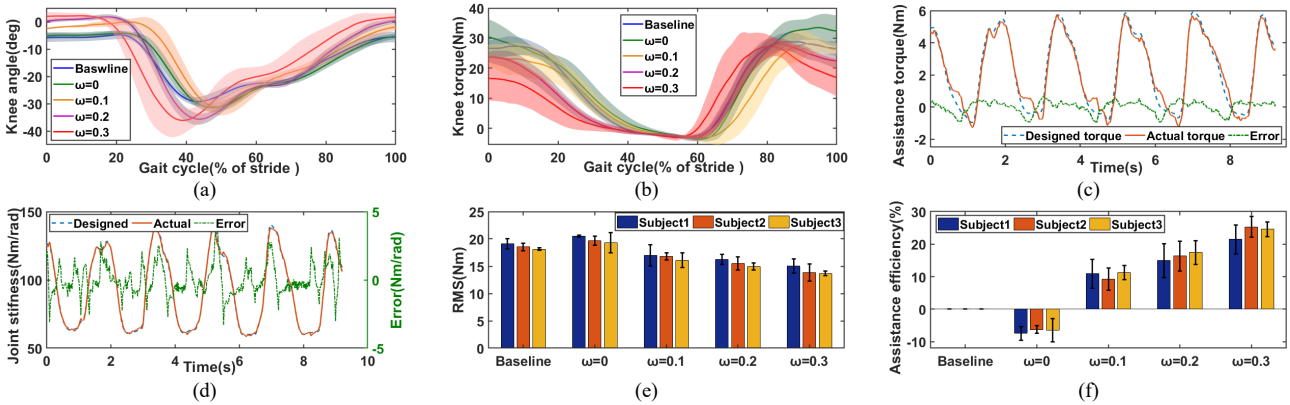

Fig.9 The results of voluntary gait assisted experiments. (a) Subject 1's knee joint angle during the gait cycle (Mean±SD); (b) Subject 1's knee joint torque estimated by sEMG during the gait cycle; (c) The designed assistance torque and actual assistance torque of the exoskeleton in the experiment of Subject 1 with the auxiliary ratio ω=0.2; (d) The design stiffness and actual stiffness of the exoskeleton in the experiment of Subject 1 with the auxiliary ratio ω=0.2; (e) The RMS of three subjects in different experiments (Mean±SD); (f) The assistance efficiency of three subjects in different experiments (Mean±SD).

TABLE IV
THE RMS AND ASSIST EFFICIENCY OF THREE SUBJECTS IN DIFFERENT EXPERIMENTS

Subject	Auxiliary ratio ω	RMS(Nm)	Assistance efficiency (%)
Subject1	Baseline	19.1004±0.9252	0
	ω=0	20.5269±0.2036	-7.47±2.15
	ω=0.1	17.0152±1.9460	10.92±4.45
	ω=0.2	16.2518±0.9221	14.91±5.23
	ω=0.3	15.0040±1.2952	21.45±4.40
Subject2	Baseline	18.5234±0.6534	0
	ω=0	19.6811±0.8256	-6.25±1.23
	ω=0.1	16.8174±0.6254	9.21±3.38
	ω=0.2	15.5004±1.2365	16.32±4.53
	ω=0.3	13.8333±1.5645	25.32±3.15
Subject3	Baseline	18.1431±0.2156	0
	ω=0	19.3242±1.8624	-6.51±3.54
	ω=0.1	16.1093±1.2984	11.21±2.15
	ω=0.2	14.9826±0.6542	17.42±3.61
	ω=0.3	13.6872±0.3987	24.56±2.20

in different experiments. It can be observed that the peak angle of the knee joint of the subject increased with the increase in the auxiliary ratio ω, but the overall gait trajectory did not change significantly. Fig. 9(b) shows the knee joint torque (mean±SD) of subject 1 in a single gait cycle. Compared with the baseline experiment, the subjects' knee joint peak torque decreased with the increase of the auxiliary ratio ω. Fig. 9(c) and Fig. 9(d) show the results of exoskeleton torque control and exoskeleton stiffness control for the five gait cycles of subject 1 when the auxiliary ratio ω=0.2, respectively, where the actual assist torque and the actual assist torque Stiffness is calculated by (1) and (2). From the results, the control error of the exoskeleton torque and stiffness is very small, indicating that the exoskeleton can accurately control the output torque and stiffness of the exoskeleton.

The statistical results of different subjects in multiple gait cycles are shown in Fig. 9(e) and Fig. 9(f), and are listed in Table IV. When the auxiliary ratio ω=0, the assistance efficiency of the exoskeleton is negative, because the mass of the exoskeleton increases the energy consumption of the subjects. However, the assistance efficiency of the three subjects is greater than -7.47%, indicating that the exoskeleton will not cause significant interference to the subject when it does not assist the subject. The statistical results show that the assistance efficiency of the exoskeleton to the three subjects increases with the increase of the auxiliary ratio ω. In addition, when the auxiliary ratio ω=0.3, the assistance efficiency of subject 2 reached 25.32%, indicating that the exoskeleton assistance can reduce the strength requirements of the subject to walk.

V. DISCUSSION

This paper proposes a sEMG-driven musculoskeletal model that predicts a subject's instantaneous joint torque and quasi-stiffness and applies these predictions to the control of the exoskeleton. The calibrated experimental results (Fig. 8 and Table III) demonstrate that the proposed sEMG-driven musculoskeletal model can accurately estimate the joint torque of different subjects. But for patients with severe movement disorders, it is still a huge challenge to estimate joint torque by capturing and processing their sEMG signals.

In the stiffness adjustment strategy of the exoskeleton, we expect to the exoskeleton to imitate the stiffness adjustment skills of humans to reduce the impact with the ground and reduce energy consumption [17]-[18]. However, how to determine the optimal stiffness parameters to achieve the optimal performance is still the goal of future research. In the torque assist strategy of exoskeleton, we implement assistance by scaling down the estimated human joint torque, which is also applicable to the exoskeleton with controllable torque (SEA or VSA driven exoskeleton). From the experimental results (Fig. 9 and Table IV) show that the subjects' peak torque and torque RMS have been reduced, and the subject's RMS decreases as the auxiliary ratio increases, which is very beneficial for patients with motor dysfunction. Compared with the non-wearing exoskeleton, the assistance efficiency of subject 2 is as high as 25.32% (ω=0.3). It is worth noting that when the auxiliary ratio continues to increase, the joint torque of the subject will decrease, resulting in a decrease in the assist torque of the exoskeleton. Therefore, the boosting effect of the exoskeleton does not always increase as the auxiliary ratio increases. Compared with healthy subjects, patients with lower muscle strength should increase the auxiliary ratio to improve assistance efficiency. However, the study has limitation, it is only applicable to patients with certain mobility. This control strategy is not suitable for some subjects without muscle strength.

VI. Conclusion

This paper proposes a variable stiffness lower extremity exoskeleton system (VSA-EXO), and conducts some feasibility experiments on healthy subjects. First, the structural design of the VSA-EXO is introduced in this paper. Then, through the biomechanical analysis of the joints, a sEMG-driven musculoskeletal model is established to estimate the torque and stiffness of the human joints. In addition, based on the established musculoskeletal model, a voluntary control strategy is proposed. In the voluntary control strategy, the exoskeleton can provide proportional assistance according to the subject's voluntary effort, and the exoskeleton can change the output stiffness of the exoskeleton according to the subject's behavior. Finally, a musculoskeletal model calibration experiment and a gait assisted experiment are carried out on three healthy subjects. The experimental results show that the proposed voluntary control strategy can achieve effective assistance. Future research will be devoted to clinical rehabilitation experiments for patients with motor dysfunction.

Appendix

The detailed expression of equation (2) is

$$\begin{aligned} K_\theta &= 4N^2Kac\cos\theta(1-(a-c)(a^2+c^2-2ac\cos\theta)^{-1/2}) \\ &+4N^2Ka^2c^2(a-c)\sin^2\theta(a^2+c^2-2ac\cos\theta)^{-3/2} \\ &+2NF_0ac\cos\theta(a^2+c^2-2ac\cos\theta)^{-1/2} \\ &-2NF_0a^2c^2\sin\theta(a^2+c^2-2ac\cos\theta)^{-3/2} \end{aligned} \tag{25}$$

References

[1] T. Xue, Z. Wang, T. Zhang and M. Zhang, "Adaptive Oscillator-Based Robust Control for Flexible Hip Assistive Exoskeleton," *IEEE Robot. Autom. Lett.*, vol. 4, no. 4, pp. 3318-3323, Oct. 2019.

[2] J. K. Mehr et al, "Intelligent Locomotion Planning With Enhanced Postural Stability for Lower-Limb Exoskeletons," *IEEE Robot. Autom. Lett.*, vol. 6, no. 4, pp. 7588-7595, Oct. 2021.

[3] G. Aguirre-Ollinger and H. Yu, "Lower-Limb Exoskeleton With Variable-Structure Series Elastic Actuators: Phase-Synchronized Force Control for Gait Asymmetry Correction," *IEEE Trans. Robot.*, vol. 37, no. 3, pp. 763-779, June 2021.

[4] Y. Zhuang, S. W. Yao, C. M. Ma and R. Song, "Admittance Control Based on EMG-Driven Musculoskeletal Model Improves the Human–Robot Synchronization," *IEEE Trans. Ind. Informat.*, vol. 15, no. 2, pp. 1211–1218, Feb. 2019.

[5] A. Esquenazi, M.Talaty, A. Packel, and M. Saulino, "The ReWalk powered exoskeleton to restore ambulatory function to individuals with thoracic-level motor-complete spinal cord injury," *Amer. J. Phys. Med. Rehabil*., vol. 91, no. 11, pp. 911–921, Nov. 2012.

[6] Di Shi, Wuxiang Zhang, and Xilun Ding, "A Review on Lower Limb Rehabilitation Exoskeleton Robots," *Chin. J. Mech. Eng.*, vol.32, no.1, Aug. 2019, Art. no.74.

[7] K. A. Strausser and H. Kazerooni, "The development and testing of a human machine interface for a mobile medical exoskeleton," i*n Proc. IEEE/RSJ Int. Conf. Intell. Robots Syst.*, 2011, pp. 4911–4916.

[8] G. Lv, H. Zhu, and R. D. Gregg, "On the design and control of highly back drivable lower-limb exoskeletons: A discussion of past and ongoing work," *IEEE Control Syst.*, vol. 38, no. 6, pp. 88–113, Dec. 2018.

[9] P. Herbin, M. Pajor, "Human-robot cooperative control system based on serial elastic actuator Bowden cable drive in ExoArm 7-DOF upper extremity exoskeleton," *Mech. Mach. Theory*, vol. 163, Sep. 2021, Art. no.104372.

[10] T. Bacek *et al*., "Varying mechanical compliance benefits energy efficiency of a knee joint actuator," *Mechatronics*, vol. 66, Arp. 2020, Art. no. 102318.

[11] S. Wolf *et al*., "Variable Stiffness Actuators: Review on Design and Components," *IEEE/ASME Trans. Mechatronics*, vol. 21, no. 5, pp. 2418-2430, Oct. 2016.

[12] B. Ugurlu *et al*., "Variable Ankle Stiffness Improves Balance Control: Experiments on a Bipedal Exoskeleton," *IEEE/ASME Trans. Mechatronics*, vol. 21, no. 1, pp. 79-87, Feb. 2016.

[13] Y. Shao *et al*., "Design and optimisation of load-adaptive actuator with variable stiffness for compact ankle exoskeleton," *Mech. Mach. Theory*, vol.161, Jul. 2021, Art. no.104323.

[14] L. Liu, "Experimental validation of a torque-controlled variable stiffness actuator tuned by gain scheduling," *IEEE/ASME Trans. Mechatronics*, vol. 23, no. 5, pp. 2109–2120, Oct. 2018.

[15] Z. Li, S. Bai, O. Madsen, W. Chen, and J. Zhang, "Design, modeling and testing of a compact variable stiffness mechanism for exoskeletons," *Mech. Mach. Theory*, vol. 151, Sep. 2020, Art. no.103905.

[16] Y. Zhu, Q. Wu, B. Chen, D. Xu and Z. Shao, "Design and Evaluation of a Novel Torque-Controllable Variable Stiffness Actuator with Reconfigurability," *IEEE/ASME Trans. Mechatronics*, doi: 10.1109/TMECH.2021.3063374.

[17] S. O. Schrade *et al*., "Knee Compliance Reduces Peak Swing Phase Collision Forces in a Lower-Limb Exoskeleton Leg: A Test Bench Evaluation," *IEEE Trans. Biomed. Eng.*, vol. 68, no. 2, pp. 535-544, Feb. 2021.

[18] F. Russell, Y. Takeda, P. Kormushev, R. Vaidyanathan and P. Ellison, "Stiffness Modulation in a Humanoid Robotic Leg and Knee," *IEEE Robot. Autom. Lett.*, vol. 6, no. 2, pp. 2563-2570, Apr. 2021.

[19] T. Yan, M. Cempini, C. M. Oddo, and N. Vitiello, "Review of assistive strategies in powered lower-limb orthoses and exoskeletons," *Robot. Auton. Syst.*, vol. 64, pp. 120–136, Feb. 2015.

[20] X. Li, Q. Yang and R. Song, "Performance-Based Hybrid Control of a Cable-Driven Upper-Limb Rehabilitation Robot," *IEEE Trans. Biomed. Eng.*, vol. 68, no. 4, pp. 1351-1359, Apr. 2021.

[21] H. J. Asl, M. Yamashita, T. Narikiyo and M. Kawanishi, "Field-Based Assist-as-Needed Control Schemes for Rehabilitation Robots," *IEEE/ASME Trans. Mechatronics*, vol. 25, no. 4, pp. 2100-2111, Aug. 2020.

[22] S. Hussain, S. Q. Xie and P. K. Jamwal, "Adaptive Impedance Control of a Robotic Orthosis for Gait Rehabilitation," *IEEE Trans. Cybern.*, vol. 43, no. 3, pp. 1025-1034, June 2013.

[23] K. Gui, U. Tan, H. Liu and D. Zhang, "Electromyography-Driven Progressive Assist-as-Needed Control for Lower Limb Exoskeleton," *IEEE Trans. Med. Robo. Bionics*, vol. 2, no. 1, pp. 50-58, Feb. 2020.

[24] C. Caulcrick, W. Huo, W. Hoult and R. Vaidyanathan, "Human Joint Torque Modelling With MMG and EMG During Lower Limb Human-Exoskeleton Interaction," *IEEE Robot. Autom. Lett.*, vol. 6, no. 4, pp. 7185-7192, Oct. 2021.

[25] B. Huang et al, "Coordination Control of a Dual-Arm Exoskeleton Robot Using Human Impedance Transfer Skills," *IEEE Trans. Syst., Man, Cybern., Syst.*, vol. 49, no. 5, pp. 954-963, May 2019.

[26] Florian L. Haufe *et al*., "Biomechanical effects of passive hip springs during walking," *J. Biomech.*, vol.98, Jan.2020, Art. no.109432.

[27] Fausto A. Panizzolo1et al., "Reducing the energy cost of walking in older adults using a passive hip flexion device," *J. NeuroEng. Rehabil.*, vol.16, no.1, Oct. 2019, Art. no..117.

[28] C. Fleischer, "A Human-Exoskeleton Interface Utilizing Electromyography," *IEEE Trans. Robot,* vol. 24, no. 4, pp. 872–882, Aug. 2008.

[29] S. L. Delp *et al*., "OpenSim: Open-source software to create and analyze dynamic simulations of movement," *IEEE Trans. Biomed. Eng.*, vol. 54, no. 11, pp. 1940–1950, Nov. 2007.

[30] Z. Li, Y. Kang, Z. Xiao and W. Song, "Human–Robot Coordination Control of Robotic Exoskeletons by Skill Transfers," *IEEE Trans. Ind. Electron.*, vol. 64, no. 6, pp. 5171-5181, Jun. 2017.

[31] F. Petit and A. Albu-Schaffer, "Cartesian impedance control for a variable stiffness robot arm," in Proc. IEEE/RSJ Int. Conf. Intell. Robot. Syst., Sep. 2011, pp. 4180–4186.

[32] Wei Meng *et al*., "Recent development of mechanisms and control strategies for robot-assisted lower limb rehabilitation," *Mechatronics*, vol. 31, pp.132-145, Oct. 2015.

[33] F. Edition and David A. Winter, Biomechanics and motor control of human movement, vol. 28, no. 04. 1990